Evaluation of crack resistance of CrSiCN coatings as a function of Si concentration via nanoindentation

Qianzhi Wang [a], Zhiwei Wu [b,c], Fei Zhou [b,c,*], Hu Huang [a], Keiichiro Niitsu [a], Jiwang Yan [a,**]

[a] Department of Mechanical Engineering, Faculty of Science and Technology, Keio University, Yokohama 2238522, Japan
[b] College of Mechanical and Electrical Engineering, Nanjing University of Aeronautics and Astronautics, Nanjing 210016, China
[c] Jiangsu Key Laboratory of Precision and Micro-Manufacturing Technology, Nanjing 210016, China

ARTICLE INFO

ABSTRACT

A series of CrSiCN coatings with various Si concentrations were deposited on Si(100) wafers, and the influence of Si content on the microstructure, mechanical property and crack resistance of the coatings was investigated by XRD, Raman spectroscopy and nanoindentation. After introducing $(CH_3)_3SiH$ into precursor from 5 sccm to 30 sccm, the Si concentration increased from 0.97 at.% to 7.00 at.% with gradually increasing formation of amorphous SiC_x and SiN_x. Under low Si concentration (0.97–3.40 at.%) condition, solid solution effect and formation of nc-Cr(C,N)/a-SiN_x(a-SiC_x) architecture caused an increase in hardness from 18.1 GPa to 21.3 GPa. In contrast, at high Si concentration (5.35–7.00 at.%), larger grain separation, which resulted from the increase of a-SiN_x(a-SiC_x), led to a drop of hardness to a low range of 13.0–13.6 GPa and a decrease in compressive stress from 4.74 GPa to 2.78 GPa. As a result, superior elasticity and high compressive stress prevented the CrSiCN (Si < 3.40 at.%) coatings from radial crack, whereas the CrSiCN (Si ≥ 3.40 at.%) coatings confronted. However, after unloading, unbalance of high compressive stress (4.74 and 4.83 GPa) in CrCN and CrSiCN (0.97 at.%) coatings initiated cracks parallel to the indenter edge. On account of favorable H/E, H^3/E^2 and compressive stress, the CrSiCN coating with 2.05 at.% Si presented the best mechanical property and crack resistance.

© 2015 Elsevier B.V. All rights reserved.

1. Introduction

CrN coatings have superior mechanical and corrosion-proof properties, and are regarded as potential substitutes for TiN coatings, which have been successfully employed to protect cutting tools and molding dies [1–6]. However, low hardness of CrN coatings stands in its way of wide application, especially in tribology, where hardness is a crucial parameter [7,8]. Many researchers have attempted to enhance the hardness of CrN coatings by introducing metal (Ti, Al, W) [9–11] or nonmetal (Si, C, B) elements [12–14]. Among these elements, carbon has been adopted frequently due to its excellent self-lubrication ability. Hu et al. [15] revealed that carbon incorporation (46.43 at.%) could raise the hardness of CrCN coatings to 2300 Hv. Likewise, by 20.00 at.% carbon addition, an increase of 6 GPa in hardness was reported in Ref. [16]. Accordingly, these CrCN coatings perform more preferable tribology than binary CrN coatings [15–17]. Nonetheless, Fuentes et al. [18] and Warcholinski's group [19–22] pointed out that, even though the hardness of CrCN coatings increased, their residual stress also rose to a

certain extent. Subsequently, higher residual stress led to poor adhesion to substrate, and deteriorated the tribology of CrCN coatings [19–21]. On the other hand, compared with CrN coatings, CrCN coatings present higher surface roughness due to higher microparticle density [23]. Thus, it is of paramount importance to restrain residual stress and refine grain size of CrCN coatings. So far, surface refinement of CrCN coatings by doping Si has been demonstrated in Refs. [24,25], while the adhesive strength of CrSiCN coatings can reach up to 42–45 N in Refs. [26,27]. In addition, Jeon et al. [28] reported a reduction of friction coefficient for CrCN coatings via Si alloying. However, previous investigations either studied corrosion behavior alone [24,25], or just focused on a singular Si concentration [26,27]. No attention has been paid on the residual stress and crack resistance of CrSiCN coatings, especially the influence of Si concentration on the grain size, residual stress, mechanical property and crack resistance of the coatings.

In this study, the effect of Si concentration on microstructure, surface roughness, residual stress, elasticity and crack resistance of CrSiCN coatings was investigated by using XRD, Raman spectroscopy, white-light interferometer, nanoindentation and Field-Emission Scanning Electron Microscope (FE-SEM). Moreover, the correlation among microstructure, mechanical property and crack resistance was elucidated.

* Corresponding author. Tel./fax: +86 25 8489 3083.
** Corresponding author. Tel.: +81 45 566 1445; fax: +81 45 566 1495.
E-mail addresses: fzhou@nuaa.edu.cn (F. Zhou), yan@mech.keio.ac.jp (J. Yan).

2. Experimental details

2.1. Fabrication of coatings

After ultrasonic bath in ethanol and deionized water, monocrystal Si(100) wafer (H = 12.4 GPa, E = 198 GPa, t_s = 525 ± 20 μm) was attached on the turntable in vacuum chamber of Closed-Field Unbalanced Magnetron Sputtering system (UDP-650, Teer Coatings Limited, UK). Prior to coating fabrication, a 30 min. lasting bombardment of Ar^+ plasma at bias voltage of −450 V was carried out for intensively cleaning and activating Si(100) wafer. Subsequently, in pure Ar atmosphere, a pure Cr adhesive layer (0.4 μm) was deposited firstly, and then, coupled with sputtering Cr and C targets at 1 A and 4 A, a series of CrSiCN coatings were deposited in compound precursor of Ar, N_2 and trimethylsilane (known as TMS) gases under constant pressure of 0.23 Pa. The bias voltage and rotating speed of holder were set as −60 V and 10 rpm, respectively. Through adjusting flow of TMS, Si concentration in coatings was controlled, and CrCN, CrSiCN(5), CrSiCN(10), CrSiCN(15), CrSiCN(20), CrSiCN(25), and CrSiCN(30) would be used to symbolize as coatings synthesized with TMS at 0 sccm, 5 sccm, 10 sccm, 15 sccm, 20 sccm, 25 sccm, and 30 sccm in the following main text.

2.2. Microstructure and residual stress of coatings

The crystal orientation of coatings was detected via X-ray diffraction (Ultima IV, Japan) at 40 kV and 40 mA. 2θ data was recorded from 20° to 80° with sampling pitch of 0.01 and scan rate of 5°/min. The amorphous feature of coatings was analyzed by Raman spectroscopy (NRS-3100, JASCO Co. Ltd., Japan). Moreover, the thickness and composition of coatings were observed and quantified by Field-Emission Scanning Electron Microscope (JEOL-JSM-7001F) with additional EDS (Inca Energy 350, Oxford, UK), and relevant results are listed in Table 1.

As seen in Fig. 1, the contours of Si wafers before and after coating were measured by non-contact white-light interferometer (CCI 3D, Taylor Hobson Ltd. UK), and the upward bending phenomenon is a typical result caused by compressive stress after coating. The individual width (a) and height (h) of each contour were measured, and then individual radius of curvature (R) can be obtained via R = a^2 + h^2 / 2 h. Subsequently, according to Stoney's formula (1), the compressive stress of coatings (σ_c) can be calculated [29–31]:

$$\sigma_c = \frac{1}{6} \frac{E_s t_s^2}{(1 - \nu_s) t_c} \left(\frac{1}{R_2} - \frac{1}{R_1} \right) \tag{1}$$

where E_s, ν_s and t_s are the elastic modulus, Poisson ratio (0.27) and thickness of silicon wafer, while t_c is the thickness of coatings. In addition, R_1 and R_2 are the radiuses of curvature before and after coatings deposition.

2.3. Mechanical properties of coatings

The hardness (H) and elastic modulus (E) of coatings were measured by nanoindentation (ENT-1100a, Elionix Co. Ltd.) with Berkovich

Table 1
Thickness and element concentration of CrSiCN coatings at different TMS flows via SEM and EDS.

| Coatings	Thickness (μm)	Sa (nm)	Cr (at.%)	Si (at.%)	C (at.%)	N (at.%)
CrCN	2.00	4.33	48.75	0	8.72	42.53
CrSiCN(5)	1.84	4.72	44.81	0.97	9.25	44.98
CrSiCN(10)	1.96	4.31	42.48	2.05	13.47	42.00
CrSiCN(15)	1.93	4.55	50.49	3.40	16.15	29.96
CrSiCN(20)	1.84	3.15	52.33	5.35	25.30	17.02
CrSiCN(25)	1.99	3.28	55.57	6.20	29.50	8.74
CrSiCN(30)	1.97	3.16	53.49	7.00	33.44	6.07
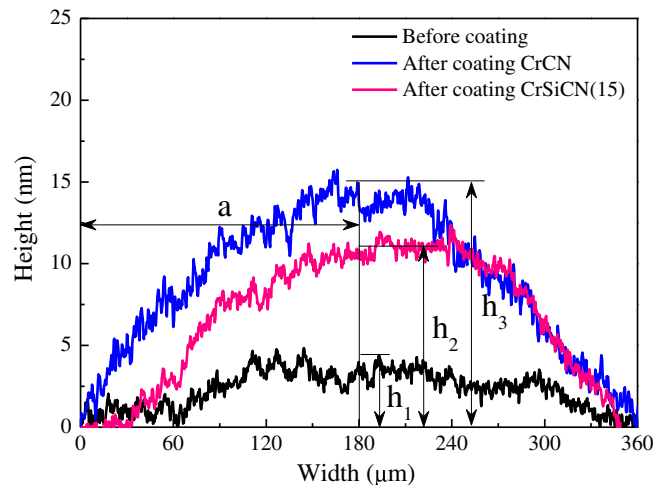
Fig. 1. Cross-sectional contour of Si wafer before and after coating.

indenter made of single crystal diamond. Tests were performed at constant penetration depth of 100 nm to minimize substrate effect, and 36 nanoindentations were conducted at room temperature to ensure reliability of data. After nanoindentation tests, individual H/E, H^3/E^2 and average elastic recovery were calculated. At last, 1000 mN was loaded on each sample via nanoindentation, and corresponding morphology of impression was observed via Field-Emission Scanning Electron Microscope (FEI-SIRION 200, Netherland) to analyze the crack phenomena of coatings.

3. Results and discussion

3.1. Composition and microstructure of coatings

Obviously, increasing flow of TMS in precursor promotes Si concentration from 0.97 at.% to 7.00 at.% as well as C concentration from 8.72 at.% to 33.44 at.%. On the contrary, concentration of N declines from 44.98 at.% to 6.07 at.% (Table 1). Even with different compositions, deposition rate is almost identical according to similar thickness around 1.9 μm under the same deposition time. The crystal orientation of CrSiCN coatings as a function of Si concentration is illustrated in Fig. 2. Besides Cr(210) adhesive layer and $Cr_{23}C_6$(511) peak at about 44°, all
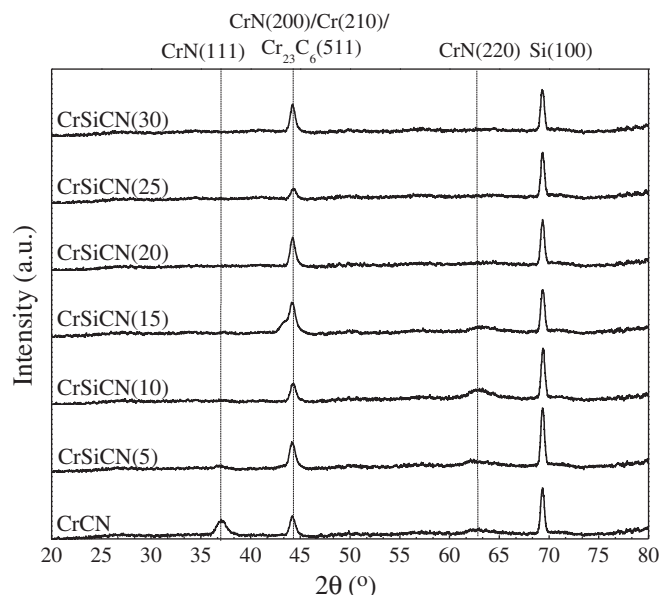
Fig. 2. X-ray diffraction of CrSiCN coatings at different flows of TMS.

samples exhibit F.C.C. crystal structure (JCPDS 11-0065, JCPDS 19-0323 and JCPDS 35-0783). As Si content increases to 2.05 at.% and 5.35 at.%, the (111) and (220) orientations of CrN disappear in CrSiCN(10) and CrSiCN(20) coatings, respectively. When Si content varies in the range of 6.20 at.% to 7.00 at.%, only one peak related to CrN(200), Cr(210) and $Cr_{23}C_6$(511) exhibits in XRD of CrSiCN(25) and CrSiCN(30) coatings. It is indicated that the incorporation of Si can promote growth of CrN(200) preferred orientation. On the other hand, there is no crystal peak of SiC(Si_3N_4), which implies that Si may exist in the forms of amorphous SiC_x and SiN_x.

In order to prove the above deduction, Raman spectra of the coatings are illustrated in Fig. 3. Overall, spectra of all the samples exhibit broad peaks with extremely low intensity, which indicates the amorphous feature of coatings. Without Si doping, the Raman spectrum of CrCN coating exhibits D peak (disorder) at 1445 cm^{-1}, G peak (graphitic) at 1570 cm^{-1}, and a shoulder peak around 570 cm^{-1}, which is attributed to overlap of Cr_2O_3 at 547 cm^{-1} and 609 cm^{-1} [32–35]. After alloying Si with 0.97 at.%, a portion of C bonds with Si, and hence the intensities of D and G peaks become weaker. With increasing Si concentration from 2.05 at.% to 5.35 at.%, the summit of shoulder peak shifts from 570 cm^{-1} to 535 cm^{-1} gradually. In the meantime, D and G peaks disappear. It is implied that carbon is prone to bond with Si rather than abundant to form amorphous carbon, and the shoulder peak around 535 cm^{-1} is ascribed to overlap of a-SiC_x (521 cm^{-1}) and Cr_2O_3 (547 cm^{-1}). In addition, alloying Si also reacts with N to form a-SiN_x at 1052 cm^{-1} [36,37]. Further increasing Si content from 6.20 at.% to 7.00 at.%, as seen in Fig. 4, higher increasing rate of C in CrSiCN(25) and CrSiCN(30) makes it rich enough to form amorphous carbon, so that D and G peaks display again in Raman spectra. Moreover, the broad peaks of a-SiC_x at 521 cm^{-1} and a-SiN_x at 1052 cm^{-1} still exist [38,39]. Thus, taking XRD and Raman spectra into account, it is confirmed that Si exists in CrSiCN coatings in the forms of a-SiC_x or a-SiN_x, and the content of a-SiC_x or a-SiN_x increases gradually as a function of Si concentration.

3.2. Mechanical properties of coatings

The mechanical properties of coatings are strongly dependent on individual microstructure. After alloying 0.97 at.% and 2.05 at.% Si, the hardness of CrSiCN(5) and CrSiCN(10) coatings raises gradually to 21.3 GPa from 18.1 GPa (Table 2). Generally, under low element doping condition, the insertion of atom prefers to seize the interstitial or
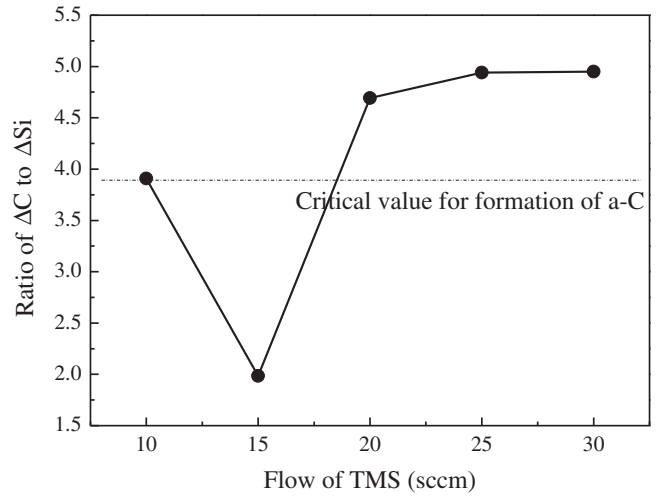

Fig. 4. Ratio of increasing C to increasing Si of CrSiCN coatings at different flows of TMS.

substitutional position of matrix atom, and then suppresses the motion of dislocation [40,41]. Thus, the enhancement of hardness for CrSiCN(5) coating is attributed to this solid solution effect. Regarding the CrSiCN(10) coating, due to formation of a-SiN_x, the composite structure of nc-Cr(C,N)/a-SiN_x contributes to the increase of hardness [42]. When Si doping concentration reaches to 3.40 at.%, more a-SiC_x(a-SiN_x) enlarges the separation of grain, and hence the hardness of CrSiCN(15) drops sightly to 19.4 GPa. What is worse, much more Si alloying (5.35–7.00 at.%) i.e. much more a-SiC_x(a-SiN_x) expands grain separation continuously, and leads to sharp decline of hardness to 13.0–13.6 GPa for CrSiCN(20), CrSiCN(25) and CrSiCN(30) coatings. Taking elastic modulus into account, H/E and H^3/E^2 are listed in Table 2, and present the same variation trend as hardness. As it is known, H/E reflects elastic strain to failure while H^3/E^2 is proportional to plastic deformation resistance in one sense [43]. Thereby, the CrSiCN(5) and CrSiCN(10) coatings with higher H/E and H^3/E^2 may be of better elasticity than the rest. By contrast, CrSiCN(20), CrSiCN(25) and CrSiCN(30) coatings may exhibit worse elastic abilities due to lower H/E and H^3/E^2. It is worth noting that, as compared with high Si-containing coatings, CrSiCN(5) and CrSiCN(10) coatings present higher elastic recovery too.

As the above mentioned, more formations of a-SiC_x and a-SiN_x fill into the separation of grain as 'amorphous glue', and so as to make CrSiCN coatings become more firm [44]. For this reason, three-dimensional arithmetic average deviation (Sa) decreases as Si concentration increases (Table 1). On the other hand, this firmness feature can be indirectly proved by standard deviation of hardness in Table 2, which declines gradually.

3.3. Morphologies of nanoindentation impressions by SEM

The SEM images of indentation impressions under 1000 mN are illustrated in Figs. 5 and 6. It is obvious that the impression marks of CrCN and CrSiCN(5) coatings exhibit several cracks paralleled to impression edges, as well as some shear faults on sidewalls. However, as doping Si increases to 2.05 at.%, there is no any crack on impression mark of CrSiCN(10) coating except some shear faults. When the concentration of Si raises continuously to 3.40 at.%, it is worth noting that a short and radial crack appears on indentation mark of CrSiCN(15) coating, accompanying with two cracks along impression edge. Subsequently, under higher Si content conditions (5.35–7.00 at.%), there are no signs of shear fault and paralleled crack, but only longer radial cracks present along the mark corners of CrSiCN(20), CrSiCN(25) and CrSiCN(30) coatings.
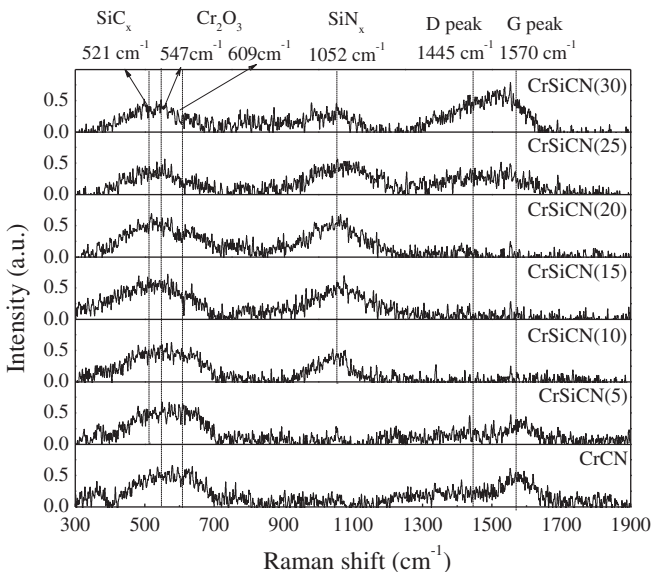

Fig. 3. Raman spectra of CrSiCN coatings at different flows of TMS.

Table 2
Mechanical properties of CrSiCN coatings at different flows of TMS via nanoindentation.

Coatings	Hardness (GPa)	Standard deviation (GPa)	Elastic modulus (GPa)	E_c/E_s	H^3/E^2 (GPa)	Elastic recovery (%)	Compressive stress (GPa)
CrCN	18.1	1.32	293	1.48	0.069	54.70	4.74
CrSiCN(5)	19.6	1.10	282	1.42	0.095	58.74	4.83
CrSiCN(10)	21.3	1.19	300	1.52	0.107	59.70	3.59
CrSiCN(15)	19.4	0.81	306	1.55	0.078	55.59	3.97
CrSiCN(20)	13.6	0.77	245	1.24	0.042	48.89	3.94
CrSiCN(25)	13.2	0.33	236	1.19	0.041	49.19	3.50
CrSiCN(30)	13.0	0.26	234	1.18	0.040	49.89	2.78

Overall, the formation and propagation of crack are a highly compli-cated process and closely related to three aspects: (1) mechanical prop-erty of the substrate; (2) microstructure, H, E, compactness of coatings; and (3) residual stress (σ_c) during coating fabrication [45,46]. In this case, because of identical substrate, the effect stemmed from mechani-cal property of Si(100) can be ignored. But the Ref. [46] made reference to ratio of elastic modulus of coatings (E_c) to substrate (E_s), and drew conclusion that the necessary condition to avoid film cracking is of a lit-tle bit higher ratio ($E_c/E_s \geq 1.3$). Thus, according to values of E_c/E_s in Table 2, CrCN, CrSiCN(5) and CrSiCN(10) coatings suppress occurrence of radial crack, whereas CrSiCN(20), CrSiCN(25) and CrSiCN(30) coat-ings suffer it. With regard to the second aspect, due to higher H/E (≥ 0.062), H^3/E^2 (≥ 0.069) and elastic recovery, CrCN, CrSiCN(5) and CrSiCN(10) coatings possess adequate elastic abilities to restrain radial cracks. The similar phenomena of Al–O–N and Zr–Al–O coatings were reported in Refs. [47,48], in which the critical value of H/E was around 0.1. By contrast, for CrSiCN(20), CrSiCN(25) and CrSiCN(30) coatings, the relatively inferior elastic abilities lead to confrontation of radial cracks. Moreover, with increasing Si content, CrSiCN(20), CrSiCN(25) and CrSiCN(30) coatings contain higher Cr and C contents in the
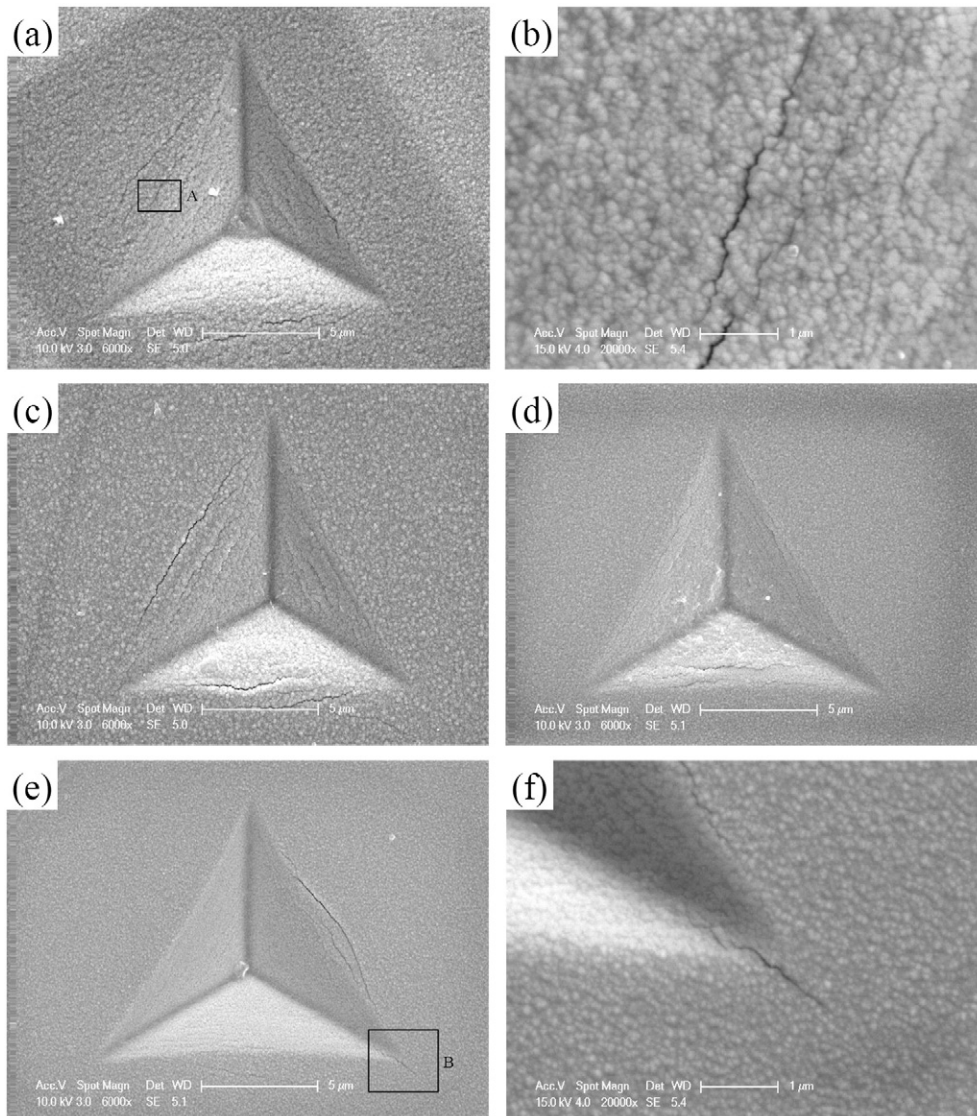

Fig. 5. Impressions of (a) CrCN, (b) Area A of CrCN, (c) CrSiCN(5), (d) CrSiCN(10), (e) CrSiCN(15) and (f) Area B of CrSiCN(15) coatings at 1000 mN.
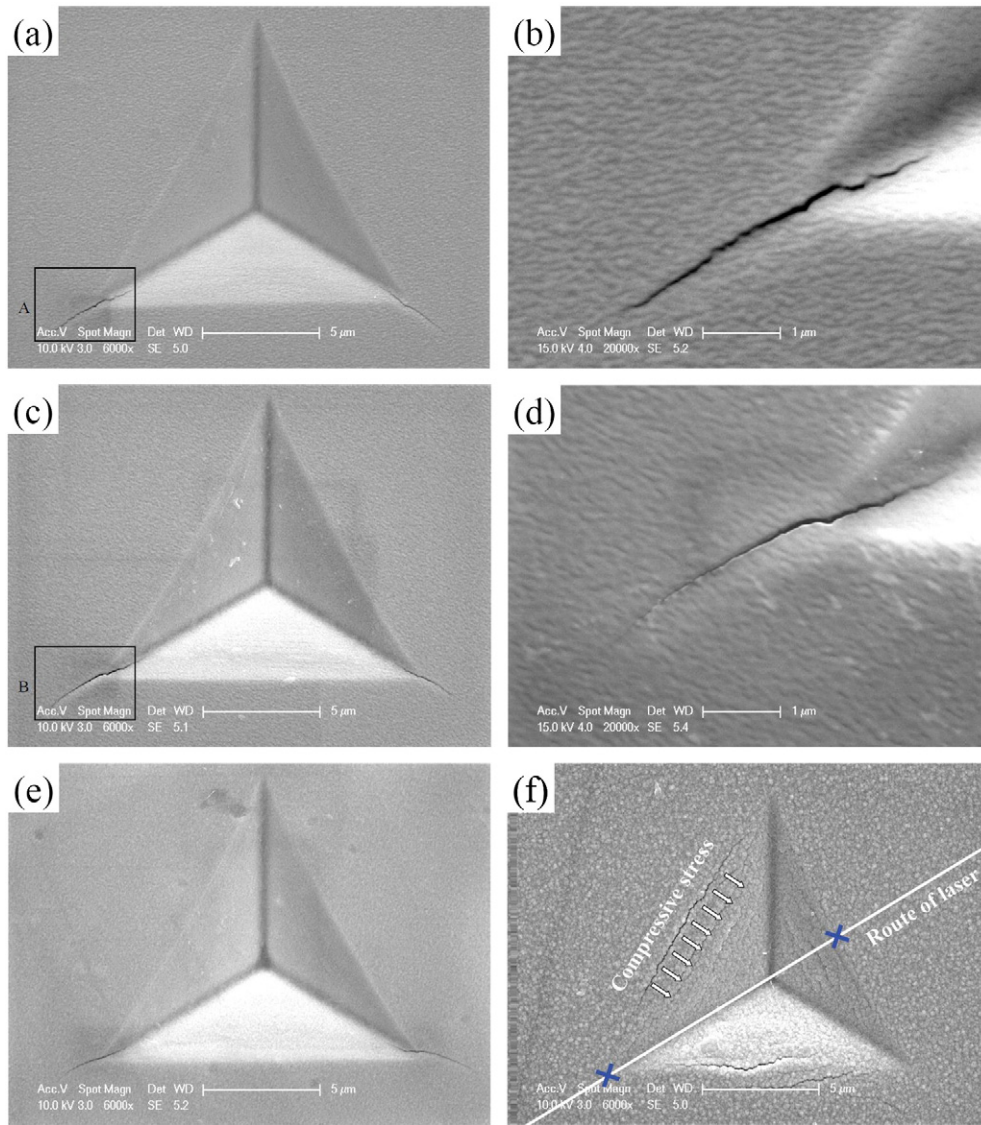
Fig. 6. Impressions of (a) CrSiCN(20), (b) Area A of CrSiCN(20), (c) CrSiCN(25), (d) Area B of CrSiCN(25), (e) CrSiCN(30) coatings at 1000 mN and (f) scanning route of laser for indentation contour and stretch by compressive stress after unloading.

meantime (Table 1). It is deduced that the content of brittle carbides such as a-SiC and $Cr_{23}C_6$ increase gradually. Dai et al. [49] and Han et al. [50] reported that brittle carbide phase like chromium carbides would reduce toughness and elastic recovery of films. Thus, at higher Si content, CrSiCN(20), CrSiCN(25) and CrSiCN(30) coatings exhibit relatively lower elastic recovery. In the same manner, the more brittle phases such as $a-SiC_x$ and $a-SiN_x$ in CrSiCN(20), CrSiCN(25) and CrSiCN(30) coatings deteriorate their crack resistance.

Although no radial crack forms on impression marks of CrCN and CrSiCN(5) coatings, the cracks paralleled to impression edge are quite special, which are attributed to two reasons. In terms of Stoney's formula, the residual stress of individual coating, compressive stress exactly, was calculated and is listed in Table 2. As the doping concentration of Si increases to 2.05 at.%, the compressive stress of CrSiCN coatings declines gradually from 4.74 GPa to 3.59 GPa. Then, the compressive stress increases slightly to 3.94 GPa in the Si concentration range of 3.40 to 5.35 at.%, while a sharp drop to 2.78 GPa when Si concentration reaches to 7.00 at.%. Musil's group [51,52] and Jungk et al. [53] reported that tensile stress of coatings promoted formation and propagation of radial crack, as opposed to compressive stress which could inhibit or shorten length of radial crack. Thus, higher compressive stress (≥4.74 GPa) of
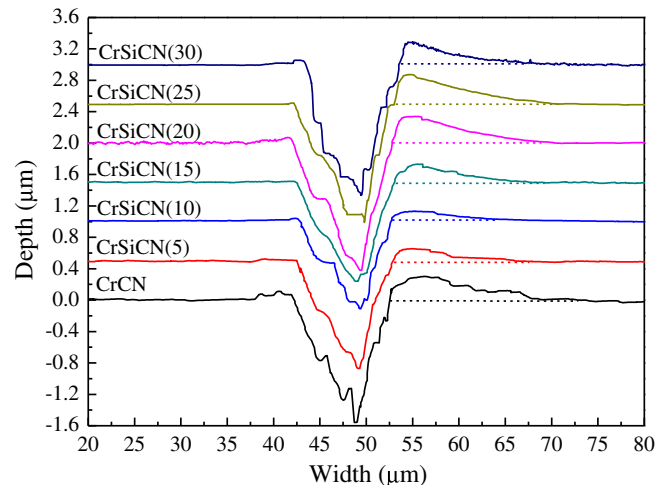
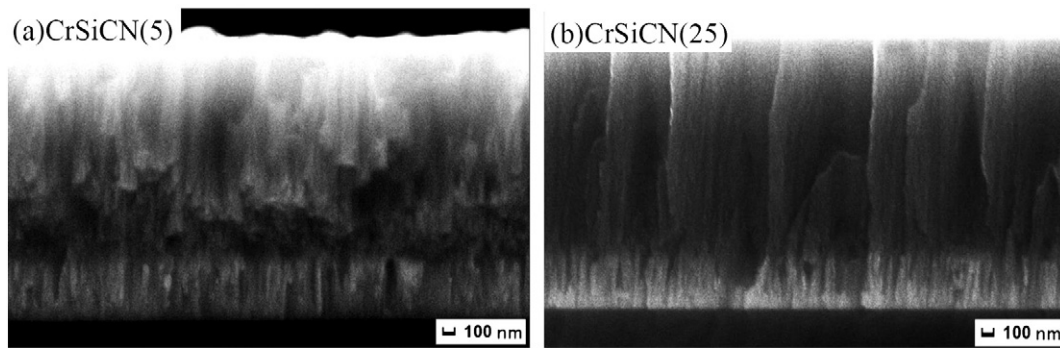**Fig. 7.** Nanoindentation contours of different CrSiCN coatings at 1000 mN.

Fig. 8. Cross-section morphologies of (a) CrSiCN(5) and (b) CrSiCN(25) coatings.

CrCN and CrSiCN(5) coating prevents the formation of radial cracks, whereas CrSiCN(15), CrSiCN(20), CrSiCN(25) and CrSiCN(30) coatings with lower compressive stress confront radial cracks easier. However, with favorable H/E (0.063), H^3/E^2 (0.078) and elastic recovery (55.59 %), the length of radial crack for CrSiCN(15) coating is much shorter than those of the rest. In addition, similar H^3/E^2 between CrCN and CrSiCN(15) coatings implies equivalent elastic strain to failure, and therefore, paralleled crack appears again on impression mark of CrSiCN(15) coating. As seen in Fig. 7, only one of the three contours is shown, with scanning route passing through one corner and the midpoint of the opposite edge (Fig. 6f). It is obvious that all of the coatings exhibit pile-up rather than sink-in, and hence the paralleled cracks of CrCN and CrSiCN(5) coatings are impossible to be induced from sink-in directly. On the contrary, after unloading, the unbalance of compressive stress along impression edge prefers to stretch the coatings toward impression center (Fig. 6f). Hence, the paralleled cracks present on impression marks of CrCN and CrSiCN(5) coatings because of higher compressive stress (around 4.74 GPa). Moreover, the incompact nature deduced from cross-section morphologies in Fig. 8 makes CrSiCN(5) coating easier to be peeled off when stretch force exists. On the contrary, a-SiN$_x$(a-SiC$_x$) as glue makes CrSiCN(25) coating become denser, and prevents peeling off when the balance of compressive stress is broken after unloading. Above all, on account of the highest H/E (0.071), H^3/E^2 (0.107), the best elastic recovery (59.70%), promising compressive stress (3.59 GPa) and modest E_c/E_s (1.52), the CrSiCN(10) coating with 2.05 at.% Si exhibits excellent resistance to crack whatever the type is.

4. Conclusions

The microstructure, mechanical properties and crack resistance of quaternary CrSiCN coatings were elucidated in this study. The conclusions are drawn as follows:

(1) As the concentration of Si increases gradually from 0.97 at.% to 7.00 at.%, amorphous SiC$_x$ and SiN$_x$ form in CrSiCN coatings, and its content increases correspondingly.

(2) The solid solution and composite architecture of nc-Cr(C,N)/a-SiN$_x$ contribute to the enhancement of hardness (18.1 GPa to 21.3 GPa) for low Si coatings (0.97 at.% and 2.05 at.%).

(3) The favorable H/E, H^3/E^2, elastic recovery and compressive stress endow CrCN, CrSiCN(5) (0.97 at.%) and CrSiCN(10) (2.05 at.%) coatings potential to inhibit radial crack, as opposed to CrSiCN coatings with Si concentration of 3.40 at.% to 7.00 at.%.

(4) The high compressive stress and incompact nature of CrCN and CrSiCN(5) (0.97 at.%) coatings lead to peeling off after unloading.

(5) The best elastic ability, modest compressive stress and compactness allow CrSiCN(10) (2.05 at.%) coating to resist radial cracks and peeling off along impression edge.

References

[1] C. Liu, Q. Bi, A. Matthews, Corros. Sci. 43 (2001) 1953–1961.
[2] M. Holzherr, M. Falz, T. Schmidt, Surf. Coat. Technol. 203 (2008) 505–509.
[3] J. Stockeme, R. Winand, P.V. Brande, Surf. Coat. Technol. 115 (1999) 230–233.
[4] A. Wilson, A. Matthews, J. Housden, R. Turner, B. Garside, Surf. Coat. Technol. 62 (1993) 600–607.
[5] W.H. Zhang, J.H. Hsieh, Surf. Coat. Technol. 130 (2000) 240–247.
[6] R. Bayon, A. Igartua, X. Fernandez, R. Martinez, R.J. Rodriguez, J.A. Garcia, A. de Frutos, M.A. Arenas, J. de Damborenea, Tribol. Int. 42 (2009) 591–599.
[7] M. Benkahoul, P. Robin, L. Martinu, J.E. Klemberg-Sapieha, Surf. Coat. Technol. 203 (2009) 934–940.
[8] E. Martinez, R. Sanjines, A. Karimi, J. Esteve, F. Levy, Surf. Coat. Technol. 180–181 (2004) 570–574.
[9] G.A. Zhang, P.X. Yan, P. Wang, Y.M. Chen, J.Y. Zhang, Appl. Surf. Sci. 253 (2007) 7353–7359.
[10] O. Knotek, F. Loffier, H.J. Scholl, Surf. Coat. Technol. 45 (1991) 53–58.
[11] Y.L. Su, T.H. Liu, Mater. Sci. Eng. A 395 (2005) 241–250.
[12] D. Mercsa, N. Bonasso, S. Naamane, J.M. Bordes, C. Coddet, Surf. Coat. Technol. 200 (2005) 403–407.
[13] Z.L. Wu, J. Lin, J.J. Moore, M.K. Lei, Thin Solid Films 520 (2012) 4264–4269.
[14] V. Jahodova, X.Z. Ding, D.H.L. Seng, W. Gulbinski, P. Louda, Thin Solid Films 544 (2013) 335–340.
[15] E.Y. Choi, M.C. Kang, D.H. Kwon, D.W. Shin, K.H. Kim, J. Mater. Process. Technol. 187–188 (2007) 566–570.
[16] P.F. Hu, B.L. Jiang, Vacuum 85 (2011) 994–998.
[17] Q.Z. Wang, F. Zhou, X.D. Ding, Z.F. Zhou, C.D. Wang, W.J. Zhang, L.K.-Y. Li, S.-T. Lee, Appl. Surf. Sci. 268 (2013) 579–587.
[18] G.G. Fuentes, M.J. Díaz de Cerio, J.A. García, R. Martínez, R. Bueno, R.J. Rodríguez, M. Rico, F. Montalá, Y. Qin, Thin Solid Films 517 (2009) 5894–5899.
[19] B. Warcholinski, A. Gilewicz, Z. Kuklinski, P. Myslinski, Surf. Coat. Technol. 204 (2010) 2289–2293.
[20] B. Warcholinski, A. Gilewicz, Z. Kuklinski, P. Myslinski, Vacuum 83 (2009) 715–718.
[21] B. Warcholinski, A. Gilewicz, Vacuum 90 (2013) 145–150.
[22] B. Warcholinski, A. Gilewicz, Plasma Process. Polym. 8 (2011) 333–339.
[23] B. Warcholinski, A. Gilewicz, J. Ratajski, Z. Kuklinski, J. Rochowicz, Vacuum 86 (2012) 1235–1239.
[24] F. Cai, X. Huang, Q. Yang, R.H. Wei, D. Nagy, Surf. Coat. Technol. 205 (2010) 182–188.
[25] F. Cai, Q. Yang, X. Huang, R.H. Wei, J. Mater. Eng. Perform. 19 (2010) 721–727.
[26] Y.J. Zheng, Y.X. Leng, X. Xin, Z.Y. Xu, F.Q. Jiang, R.H. Wei, N. Huang, Vacuum 90 (2013) 50–58.
[27] Q. Li, F.Q. Jiang, Y.X. Leng, R.H. Wei, N. Huang, Vacuum 89 (2013) 168–173.
[28] J.H. Jeon, C.S. Jang, S.Y. Yoon, B.C. Shin, K.H. Kim, Surf. Coat. Technol. 200 (2005) 1635–1639.
[29] G.G. Stoney, Proc. R. Soc. Lond. Ser. A 82 (1909) 172–175.
[30] B.J. FreundaL, A. Floro, E. Chason, Appl. Phys. Lett. 74 (1999) 1987–1989.
[31] T.L. Chou, S.Y. Yang, K.N. Chiang, Thin Solid Films 519 (2011) 7883–7894.
[32] T. Polcar, L. Cvrcek, P. Siroky, R. Novak, Vacuum 80 (2005) 113–116.

[33] J.C. Walker, I.M. Ross, C. Reinhard, W.M. Rainforth, P.Eh. Hovsepian, Wear 267 (2009) 965–975.
[34] H.C. Barshilia, K.S. Rajam, J. Mater. Res. 19 (2004) 3196–3205.
[35] C. Casiraghi, A.C. Ferrari, J. Robertson, Phys. Rev. B 72 (085401) (2005) 1–14.
[36] N. Wada, S.A. Solin, J. Non-Cryst. Solids 43 (1981) 7–15.
[37] C. Ramirez, M.I. Osendi, J. Eur. Ceram. Soc. 33 (2013) 471–477.
[38] G.S. Chung, K.S. Kim, Microelectron. J. 39 (2008) 1405–1407.
[39] S. Cichoň, P. Macháč, B. Barda, V. Machovič, P. Slepička, Thin Solid Films 520 (2012) 4378–4388.
[40] G. Kim, B. Kim, S. Lee, J. Hahn, Surf. Coat. Technol. 200 (2005) 1669–1675.
[41] Y.X. Wang, S. Zhang, Surf. Coat. Technol. 258 (2014) 1–16.
[42] S. Veprek, M.J.G. Veprek-Heijman, Surf. Coat. Technol. 202 (2008) 5063–5073.
[43] N.A. Sakharova, J.V. Fernandes, M.C. Oliveira, J.M. Antunes, J. Mater. Sci. 45 (2010) 3812–3823.
[44] S. Veprek, A. Niederhofer, K. Moto, T. Bolom, H.-D. Mannling, P. Nesladek, G. Dollinger, A. Bergmaier, Surf. Coat. Technol. 133–134 (2000) 152–159.
[45] M. Jirout, J. Musil, Surf. Coat. Technol. 200 (2006) 6792–6800.
[46] J. Musil, M. Jirout, Surf. Coat. Technol. 201 (2007) 5148–5152.
[47] J. Musil, R. Jílek, M. Meissner, T. Tölg, R. Čerstvý, Surf. Coat. Technol. 206 (2012) 4230–4234.
[48] J. Musil, J. Sklenka, R. Čerstvý, T. Suzuki, T. Mori, M. Takahashi, Surf. Coat. Technol. 207 (2012) 355–360.
[49] W. Dai, G.S. Wu, A.Y. Wang, Appl. Surf. Sci. 257 (2010) 244–248.
[50] X.X. Han, F.Y. Yan, A.M. Zhang, P.X. Yan, B. Wang, W.M. Liu, Z.X. Mu, Mater. Sci. Eng. A 348 (2003) 319–326.
[51] J. Musil, Surf. Coat. Technol. 207 (2012) 50–65.
[52] J. Blazek, J. Musil, P. Stupka, R. Cerstvy, J. Houska, Appl. Surf. Sci. 258 (2011) 1762–1767.
[53] J.M. Jungk, B.L. Boyce, T.E. Buchheit, T.A. Friedmann, D. Yang, W.W. Gerberich, Acta Mater. 54 (2006) 4043–4052.